CRYSTAL GROWTH & DESIGN

Article

Cite This: Cryst. Growth Des. 2018, 18, 242−252

pubs.acs.org/crystal

The Rich Solid-State Phase Behavior of DL-Aminoheptanoic Acid: Five Polymorphic Forms and Their Phase Transitions

Mireille M. H. Smets,[†] Mateusz B. Pitak,[‡] Joseph Cadden,[‡] Vincent R. Kip,[†] Gilles A. de Wijs,[†] Ernst R. H. van Eck,[†] Paul Tinnemans,[†] Hugo Meekes,[†] Elias Vlieg,[†] Simon J. Coles,*[,‡] and Herma M. Cuppen*[,†]

[†]Institute for Molecules and Materials, Radboud University, Heyendaalseweg 135, 6525 AJ Nijmegen, The Netherlands

[‡]Chemistry, Faculty of Natural and Environmental Sciences, University of Southampton, Highfield, Southampton, SO17 1BJ, U.K.

Supporting Information

ABSTRACT: The rich landscape of enantiotropically related polymorphic forms and their solid-state phase transitions of DL-2-aminoheptanoic acid (DL-AHE) has been explored using a range of complementary characterization techniques, and is largely exemplary of the polymorphic behavior of linear aliphatic amino acids. As many as five new polymorphic forms were found, connected by four fully reversible solid-state phase transitions. Two low temperature forms were refined in a high Z' crystal structure, which is a new phenomenon for linear aliphatic amino acids. All five structures consist of two-dimensional hydrogen-bonded bilayers interconnected by weak van der Waals interactions. The single-crystal-to-single-crystal phase transitions involve shifts of bilayers and/or conformational changes in the aliphatic chain. Compared to two similar phase transitions of the related amino acid DL-norleucine, the enthalpies of transition and NMR chemical shift differences are notably smaller in DL-aminoheptanoic acid. This is explained to be a result of both the nature of the conformational changes and the increased chain length, weakening the interactions between the bilayers.

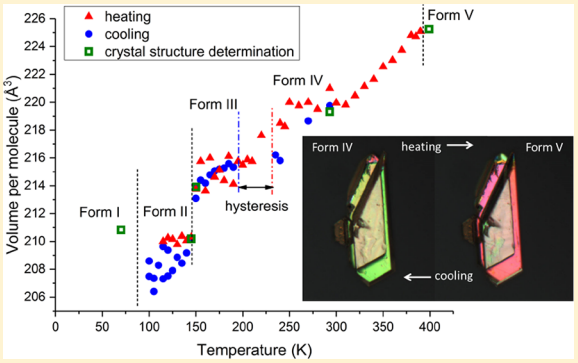

1. INTRODUCTION

Several racemates of aliphatic amino acids with an unbranched side chain have been studied in the last few decades, showing similar crystal structures and reversible temperature-dependent solid-state phase transition behavior: DL-aminobutyric acid, DL-norvaline, DL-norleucine (DL-NLE), and DL-methionine (refs 1−7 and references therein). The aliphatic amino acid molecules have a highly polar "head" and a hydrophobic side chain, resulting in amphiphilic molecules. The crystal structures of this class of molecules typically consist of two-dimensional (2D) bilayers, which are interconnected by relatively weak dispersive interactions. Their solid-state phase transitions mostly involve the translation of bilayers within the plane of the layers and often also a conformational change in the side chains.

The solid-state phase transitions of these aliphatic chain amino acids generally occur in a single-crystal-to-single-crystal fashion, although in some cases the crystal delaminates or becomes damaged during the transition. Experimental studies combined with molecular dynamics simulations on DL-NLE indicated that one of its transitions probably involves cooperative motion within the bilayers.[5,8] Cooperative or concerted motion in this context refers to a fast transition that involves the simultaneous movement of multiple molecules within one bilayer, on a limited length scale of tens or a few hundreds of molecules. To avoid confusion, this is not cooperative motion in second-order phase transitions with an infinite correlation length. In particular the solid-state NMR measurements of DL-NLE showed an increased transition rate for single crystals compared to powders. It was concluded that a cooperative mechanism was consistent with these results, since these powders contained more defects, which would slow down cooperative motion. We expect that this mechanism plays a role in the transition of similar amino acids as well. Moreover, we expect that the chain length will determine the solid-state phase behavior to a large extent. In fatty acids the melting point increases with chain length, because of increased interactions between the chains in the layers stabilizing the structure. On the other hand, a longer chain length also allows more degrees of freedom in the conformation of the molecule, thereby offering more flexibility and possibly weaker interactions between layers, which could promote entropy-driven solid-state phase transitions.

In this work, we study the crystal structures and solid-state phase transitions of an as yet unexplored aliphatic unbranched amino acid, DL-2-aminoheptanoic acid (DL-AHE, DL-homonorleucine, 145.20 g/mol), and compare its structures and solid-state phase transitions with DL-2-aminohexanoic acid (DL-NLE,

Received: August 22, 2017
Revised: November 20, 2017
Published: November 29, 2017

DOI: 10.1021/acs.cgd.7b01175
Cryst. Growth Des. 2018, 18, 242−252

DL-norleucine, 131.17 g/mol). The atomic numbering scheme used for DL-AHE is defined in Figure 1.

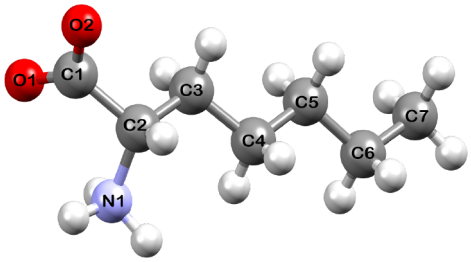

Figure 1. Atom numbering scheme of the structure of DL-AHE.

2. EXPERIMENTAL SECTION

2.1. Materials. DL-2-Aminoheptanoic acid (≤97%) was purchased from Sigma-Aldrich and used without further purification. Small high quality single crystals for single-crystal X-ray diffraction (XRD) were crystallized by antisolvent evaporation. A small vial with slightly undersaturated aqueous solution was placed in a larger vial with an acetone/water mixture as antisolvent. Slightly larger high quality single crystals, as judged by optical microscopy and X-ray diffraction, for differential scanning calorimetry (DSC) and microscopy were crystallized using hanging drop vapor diffusion in well plates. Crystals were grown in a droplet on a siliconized coverslip, which was hung upside down on top of the well plate and sealed with vacuum grease, thereby creating a closed-off reservoir below the droplet. Typically, the crystals were grown in 10 μL droplets of 4 mg/mL DL-AHE in water either using vapor diffusion of 300 μL of 10−20% ethanol or isopropanol in water as antisolvent in the reservoir, or by allowing the droplets to evaporate slowly, without any antisolvent present. Larger crystals for solid-state NMR were crystallized by allowing vapor diffusion of 30 mL of 60% ethanol in water as antisolvent from a large beaker into a small jar containing 5 mL of 3−4 mg/mL DL-AHE aqueous solution. Powder for DSC and solid-state NMR experiments was prepared by grinding crystals obtained by cooling or evaporation crystallization.

2.2. Differential Scanning Calorimetry. DSC measurements were performed using a Mettler Toledo DSC1 calorimeter with a high sensitivity sensor (HSS8), in combination with LN2 liquid nitrogen cooling, a sample robot and STAR^e software 13.00a. Powder samples and single crystals of DL-AHE were heated and cooled with rates of 2−10 K/min in the temperature range of 133−433 K. Samples of a few milligrams were sealed in an aluminum pan (40 μL), and the heat flow was measured compared to an empty reference pan as a function of temperature. The DSC was calibrated with the melting points of indium (T_{on} = 429.5 K and $\Delta_{fus}H$ = −28.13 J/g) and zinc (T_{on} = 692.85 K and $\Delta_{fus}H$ = −104.77 J/g), both supplied by Mettler Toledo.

2.3. Single Crystal X-ray Diffraction (SCXRD). Single-crystal X-ray diffraction data (DL-AHE forms II−V) were collected on a Rigaku AFC12 goniometer equipped with an enhanced sensitivity (HG) Saturn 724+ detector mounted at the window of an FR-E+ Superbright MoKα (λ = 0.71075 Å) rotating anode generator with HF Varimax optics (100 μm focus).[9] The temperature of the crystal was controlled using an Oxford Cryosystems Cobra device. For form I, single-crystal X-ray diffraction data were collected on a Crystal Logic Kappa (4 circle) goniometer equipped with a Rigaku Saturn 724+ CCD detector, using a synchrotron source (λ = 0.6889 Å) at the Diamond Light Source I-19 beamline. It was situated on an undulator insertion device with a combination of double crystal monochromator, vertical and horizontal focusing mirrors, and a series of beam slits (primary white beam and on either side of the focusing mirrors). The crystal temperature was controlled using a Helix device, and the CrystalClear[10] software package was used for instrument control and data collection.

For form I and V data reduction was performed using Rigaku CrystalClear,[10] whereas in the case of form II, III, and IV data were reduced using Rigaku CrysAlisPro suite.[11] Unit cell parameters were in all cases refined against all data. Crystal structures were solved using direct methods implemented in SHELXS[12] and refined on F_0^2 by full-matrix least-squares refinements using SHELXL[13] within the OLEX2 suite.[14] All non-hydrogen atoms were refined with anisotropic displacement parameters, except the crystal structure of form V, and all hydrogen atoms were added at calculated positions and refined using a riding model with isotropic displacement parameters based on the equivalent isotropic displacement parameter (U_{eq}) of the parent atom.

In form I, which contains six independent molecules in the asymmetric unit (Z' = 6), three independent molecules show some degree of positional disorder of the aliphatic chain. These molecules have been modeled over two sites with a 54/46, 69/31, and 51/49% ratio, respectively. Geometrical restraints DFIX and DANG were applied during structure refinement to maintain molecular geometry. SIMU, DELU, and RIGU restraints as well as EADP constraints were used to appropriately model the atomic displacement parameters.

The form V X-ray data collected at 399 K produced a heavily disordered structural model. Residual electron density around the major enantiomer component clearly indicates the presence of the second enantiomer. An approximately 10% occupation factor for this second enantiomer is a result of the phase transition at 399 K not going to completion, and this leads to a stacking fault in the structure. The $-CH(NH_3^+)COO^-$ headgroup has been modeled over two sites with 90/10% ratio of the two forms. However, the aliphatic chain group of the major component is disordered over three sites with occupancies fixed at 45%, 35%, and 20%, respectively. To maintain a reasonable molecular geometry, a number of geometrical restraints (DFIX, DANG, SAME, BIND, and FLAT) have been applied. Moreover, because of the large atomic motion at this temperature, all the disordered alkyl atoms have been refined with isotropic temperature factors, and EADP constraints were applied. All hydrogen atoms have been refined using a riding model, except H2, which was located from a difference map and geometrically restrained to the pivot carbon C2. Full crystal structure data have been deposited with CCDC deposition numbers 1563210−1563214.

2.4. Thermal Stage Polarization Microscopy. DL-AHE single crystals were studied under a nitrogen atmosphere in a Linkam LTS420 thermal stage, which was coupled to a Zeiss Axioplan 2 Imaging polarization microscope to observe the phase transitions. The microscope images were recorded with a MediaCybernetics Evolution VF digital camera. The temperature was varied between 113 and 433 K, using heating rates between 1 and 10 K/min (as indicated).

2.5. Solid-State Nuclear Magnetic Resonance. Solid-state nuclear magnetic resonance (NMR) spectra of DL-AHE were measured on a Varian VNMRS 400 MHz spectrometer, operating at a magnetic field of 9.4 T (Larmor frequencies of 399.94 MHz for ^{1}H and 100.57 MHz for ^{13}C). ^{13}C NMR spectra were measured with a Chemagnetics 3.2 mm APEX probe using ^{1}H → ^{13}C cross-polarization (CP), magic angle spinning (MAS), and SPINAL decoupling[15] for temperatures between 128 and 423 K. The powder spectra of DL-AHE mixed with KBr were recorded at an MAS frequency of 10 kHz with radio frequency (RF) field strengths of 50 kHz for ^{1}H and 60 kHz for ^{13}C during cross-polarization and 80 kHz for ^{1}H SPINAL decoupling with a pulse length of 5 μs and a phase of 6 deg.

Single crystals of DL-AHE, grown by vapor diffusion, were placed in a rotor containing KBr powder on the bottom, to ensure the single crystal was in the middle of the rotor. The rotor was then gently filled with KBr powder on top of the single crystals to obtain a well-balanced rotor for MAS. The single crystal spectra were recorded in the temperature range between 138 and 423 K at a MAS frequency of 5 kHz with RF field strengths of 58 kHz for ^{1}H and 63 kHz for ^{13}C during cross-polarization and 80 kHz for ^{1}H SPINAL decoupling with a pulse length of 7 μs and a phase of 4 degrees.

KBr was used both in powder and "single crystals" samples to adjust the magic angle setting at each temperature on the spinning side bands of ^{79}Br. Adamantane was used as reference sample for the chemical shift; the ^{13}C peak with the highest chemical shift value corresponds to the CH_2 of adamantane at 38.48 ppm. The spectra were processed using the matNMR processing package that runs under Matlab.[16]

DOI: 10.1021/acs.cgd.7b01175
Cryst. Growth Des. 2018, 18, 242−252

2.6. Density Functional Theory (DFT) Calculations. Calculations were carried out with the Vienna Ab initio Simulation Package (VASP)[17,18] at the level of density functional theory (DFT) using the projector augmented-wave (PAW) method.[19,20] The crystal structures were relaxed, starting from the experimental positions obtained by SCXRD, using the Becke Perdew Ernzerhof (PBE)[21,22] exchange-correlation functional and the DFT-D3 force field.[23] All atomic positions were optimized, whereas the unit cell parameters were kept fixed at the experimental values. For the optimized positions PBE NMR chemical shieldings were calculated with the gauge-including PAW (GIPAW) method of refs 24 and 25 as implemented in VASP.[26] The calculations were executed for form II with the conventional *C*2 unit cell. A 1 × 4 × 1 **k**-point mesh was used, including the Γ point. Standard PAW data sets as supplied with VASP were used.[27] The nonlocal projections were carried out in real space.[27,28] The kinetic energy cutoff on the Kohn−Sham states was 600 eV. Calculations on single molecules (in their crystal conformations) were carried out in large boxes of 30 × 30 × 30 Å^3 in order to minimize the effects on the shieldings of the currents induced in the periodic images.

A regression line was made for referencing of the calculated isotropic chemical shieldings σ_{iso}^{DFT} by comparing them to the experimental chemical shifts. The referencing formula for the chemical shielding of the DFT calculation is

$$\delta_{iso} = -0.959\sigma_{iso}^{DFT} + 165.6$$

Calculated ^{13}C chemical shifts δ_{iso} reported below have been calculated with this formula.

3. RESULTS AND DISCUSSION

3.1. Single Crystal X-ray Diffraction. The unit cell of DL-AHE was measured as a function of temperature in order to observe any solid-state phase transitions and to determine the temperatures at which the complete data sets for each polymorphic form should be recorded. From previous work on DL-NLE, we have experienced that some solid-state phase transitions in linear aliphatic amino acids are difficult to observe using only DSC.[4,5] Therefore, although it is quite time-consuming, we consider it necessary to perform SCXRD unit cell measurements over a large temperature range in order to find polymorphic forms and their solid-state phase transitions.

The SCXRD unit cell measurements of DL-AHE revealed that there are at least three solid-state phase transitions and therefore four polymorphic forms (II, III, IV, and V) between 100 and 400 K. SCXRD measurements at the Diamond Light Source (DLS) synchrotron revealed a fifth polymorphic form, which is named form I, since it was determined at the lowest temperature (70 K). Figure 2 shows the volume of the unit cells as a function of temperature. There is a large change in the unit cell parameters and/or symmetry below 100 K, at 146 K and at 396 K, which is emphasized by the black dashed lines in Figure 2. Furthermore, there is a change from a C-centered unit cell to a P unit cell upon heating and vice versa upon cooling, indicated by the red and blue dashed lines, respectively. On the basis of this graph, the following temperatures were chosen for structure determination: form II at 145 K, form III at 150 K, form IV at 293 K, and form V at 399 K.

The crystal structures of the five polymorphic forms of DL-AHE are described here in detail. The structures show great similarity to the known crystal structures of DL-norleucine (DL-NLE)[4] and other related aliphatic amino acids.[1,3,6,29] Because of the zwitterionic nature of the amino acid, all five forms of DL-AHE consist of strongly hydrophilic 2D LD−LD hydrogen-bonded networks,[30] forming bilayers with the hydrophobic chains arranged such that they are directed out from the center of the bilayer. These bilayers are interconnected through relatively

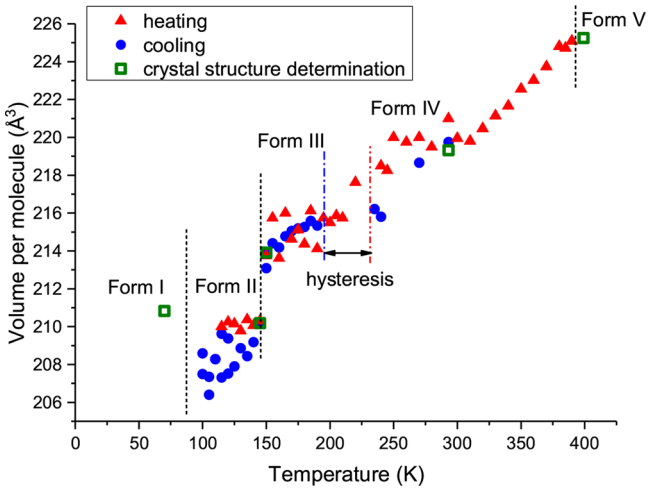

Figure 2. Volume per molecule of DL-AHE as a function of temperature as determined using SCXRD during heating (red symbols) and cooling (blue symbols) between 100 and 393 K. The green symbols indicate the volume per molecule for the full crystal structure determinations of the five polymorphic forms between 70 and 399 K. The dashed lines indicate the observed phase transition temperature at which the space group changes for forms II ↔ III (black), for III ↔ IV during cooling (blue) and heating (red), and for IV ↔ V (black).

weak dispersive (van der Waals) interactions. A crystallographic summary of the five polymorphic forms and the structure refinement details are presented in Table 1.

The crystal structures of the five polymorphic forms of DL-AHE are shown in Figures 3 and 4. The torsion angles mentioned below are for the absolute configuration *S*. The unit cell of form IV will be used as a reference to describe the structural changes for the other polymorphic forms. Form I is a $P2_1$ structure with $Z' = 6$ and disorder in the side chains of three of the molecules in the asymmetric unit. Several different conformations of the aliphatic chain are present in the crystal structure. The most common conformation is *gauche−,trans,trans,trans*. In Figure 3a alternative conformations are shown in purple, and in Figure 4a only one conformation is shown for each molecule for clarity. Form II is an ordered *C*2 structure with $Z' = 8$ and two distinct conformations of the molecules; *gauche−,trans,trans,trans* is the conformation in six molecules and *gauche−,trans,trans,gauche+* is the other conformation that systematically only occurs in two of the *S* molecules in the asymmetric unit. The unit cell axes of form II are dashed in Figures 3b and 4b, since they are too long to be displayed completely. Form III is a $C2/c$ structure and form IV a $P2_1/c$ structure, both with $Z' = 1$ and *gauche−,trans,trans,trans* conformation. Form V is a heavily disordered $C2/c$ structure with both enantiomers occupying the same position in the asymmetric unit in an approximately 90/10% ratio. This is a result of an incomplete phase transition at 399 K, which leads to the stacking fault. In the major component the alkyl chain adopts three distinct conformations (1) *gauche−,trans,gauche+,trans*, (2) *trans,trans,syn,trans*, and (3) *gauche+,trans,syn,trans*, whereas the minor component is in *syn,trans,gauche−,trans* conformation. The disorder of the major component at this considerably elevated temperature probably arises from the distance between subsequent bilayers, which becomes small (only 1.9 Å shortest H−H distance) if only the *gauche−,trans,gauche+,trans* conformation would be present. In the alternative conformations *trans,trans,syn,trans* and *gauche+,trans,syn,trans*, the aliphatic chain is more compact, thereby generating more space between

DOI: 10.1021/acs.cgd.7b01175
Cryst. Growth Des. 2018, 18, 242−252

Table 1. Spacegroup and Unit Cell Parameters for the Five Polymorphs of DL-AHE

polymorph	Form I	Form II	Form III	Form IV	Form V
Crystal Data					
CCDC deposition no.	1563211	1563213	1563210	1563214	1563212
crystal system	monoclinic	monoclinic	monoclinic	monoclinic	monoclinic
space group	$P2_1$	$C2$	$C2/c$	$P2_1/c$	$C2/c$
temperature (K)	70	145	150	293	399
a (Å)	21.38(6)	48.6095(12)	37.524(4)	18.7514(6)	38.300(5)
b (Å)	4.744(12)	4.74590(10)	4.7305(3)	4.7507(2)	4.840(5)
c (Å)	25.53(6)	36.4945(9)	9.8406(7)	9.8872(4)	9.740(5)
β (deg)	102.25(4)	126.975(2)	101.571(8)	95.106(3)	93.380(5)
V (Å^3)	2530(11)	6726.0(3)	1711.3(2)	877.29(6)	1802(2)
V per molecule (Å^3)	210.9	210.2	213.9	219.3	225.2
Z/Z'	12/6	32/8	8/1	4/1	8/1
density (calc.) (g cm^{-3})	1.143	1.147	1.127	1.099	1.070
radiation type	Synchrotron λ = 0.6889 Å	Mo Kα	Mo Kα	Mo Kα	Mo Kα
μ (mm^{-1})	0.078	0.083	0.082	0.080	0.077
Data collection					
reflections collected	20688	36432	4917	4794	5207
independent reflections	8986	11198	1511	1545	1492
R_{int}	0.166	0.080	0.025	0.028	0.063
Refinement					
R [$F^2 > 2\sigma(F^2)$]	0.115	0.066	0.057	0.051	0.149
$wR(F^2)$, S	0.431, 0.82	0.194, 1.06	0.161, 1.10	0.148, 1.06	0.477, 1.30

the bilayers. In Figure 3e the alternative conformation *trans,-trans,syn,trans* is shown in purple, and in Figure 4e only one conformation is shown for each molecule for clarity.

As can be observed in Figure 2 and Table 1, the molecular volume is larger for form I than form II. A volume increase on cooling to another polymorph contradicts the density rule and is quite rare. However, recently the same phenomenon was observed for the molecule dapsone, which also involved a small shift of molecular layers and minor conformational changes.[31] Under normal circumstances a structure contracts on cooling; however, in the case of a phase transition with a conformational change the volume occupied by the molecules can increase. In particular in amino acid layered structures there is always a trade-off between a compact structure with a higher energy conformation and a less compact structure with larger cavities.[30,32,33] The longer the aliphatic chain, the more possibilities there are for conformational changes to optimize the stacking.

The crystal structures of Forms I and II are found to be in the (noncentrosymmetric) Sohnke space groups $P2_1$ and $C2$, respectively, and therefore do not possess formal symmetry elements of the second kind, which are necessary to generate the second enantiomer of the racemic mixture. Racemates that crystallize in a Sohnke space group are also called "krypto-racemates".[34] Close inspection of the structures shows a pseudo inversion center (see Figure 3) between molecules where conformational flexibility of the aliphatic chains breaks the strict symmetry. The phenomenon of racemates crystallizing in non-centrosymmetric space groups (including also non-Sohnke) has been observed in similar materials previously and is fully studied by Dalhus and Görbitz,[35] who describe them as non-centrosymmetric racemates and document its relatively high occurrence among racemates in the CSD.[36] This is also the reason for the relatively high values of Z' for these structures (see Solid-State NMR section described later).

In general, the crystal structures differ in the stacking of the bilayers and/or the conformation of the aliphatic chains, but the hydrogen-bonding pattern remains largely unaffected. Forms I and II mainly differ in the bilayer stacking by a shift of every second bilayer over [0 $^1/_2$ $^1/_2$] with respect to the $P2_1/c$ unit cell of form IV. Furthermore, the conformations are different in both forms, although the main conformation is the same.

Forms II and III only differ in the number of molecules in the asymmetric unit and conformation. Despite a significant volume change between these two forms the stacking pattern remains the same, as is shown by the purple boxes in Figures 3b,c and 4b,c. The II → III phase transition mainly involves the change in conformation of two *S* molecules per eight DL-AHE molecules from *gauche−,trans,trans,gauche+* to *gauche−,trans,trans,trans*, as is indicated for one molecule by the green boxes in Figures 3b,c and 4b,c.

Forms III and IV have a similar conformation of the molecule *gauche−,trans,trans,trans*, but differ in the bilayer stacking by a shift of every second bilayer over [0 $^1/_2$ $^1/_2$] with respect to the $P2_1/c$ unit cell of form IV, which is indicated by the purple boxes in Figures 3c,d and 4c,d. Since there is no conformational change, both forms have a very similar volume per molecule.

The IV → V phase transition involves a packing change by a shift over [0 $^1/_2$ 0] with respect to the $P2_1/c$ unit cell of form IV, which is indicated by the purple boxes in Figure 4d,e. The conformation changes from *gauche-,trans,trans,trans* in form IV to *gauche−,trans,gauche+,trans* and *trans,trans,gauche−,trans* in form V, indicated by the green boxes in Figure 3d,e. The most likely mechanism for this transition is via a rotation in a "pedal crank"-like fashion; i.e., the rotation of the aliphatic chain (equal and opposite in the two halves of a single bilayer) enables the antiparallel slippage of adjacent bilayers. This has to occur along the C4−C5 bond for the first conformation of form V and additionally along the C2−C3 bond for the second conformation. The red boxes in Figures 3d,e show that in this way no shift over [0 0 $^1/_2$] is necessary during the phase transition.

3.2. Differential Scanning Calorimetry. The solid-state phase transitions of DL-AHE have been characterized using DSC by determining the transition temperatures, the enthalpies of

DOI: 10.1021/acs.cgd.7b01175
Cryst. Growth Des. 2018, 18, 242−252

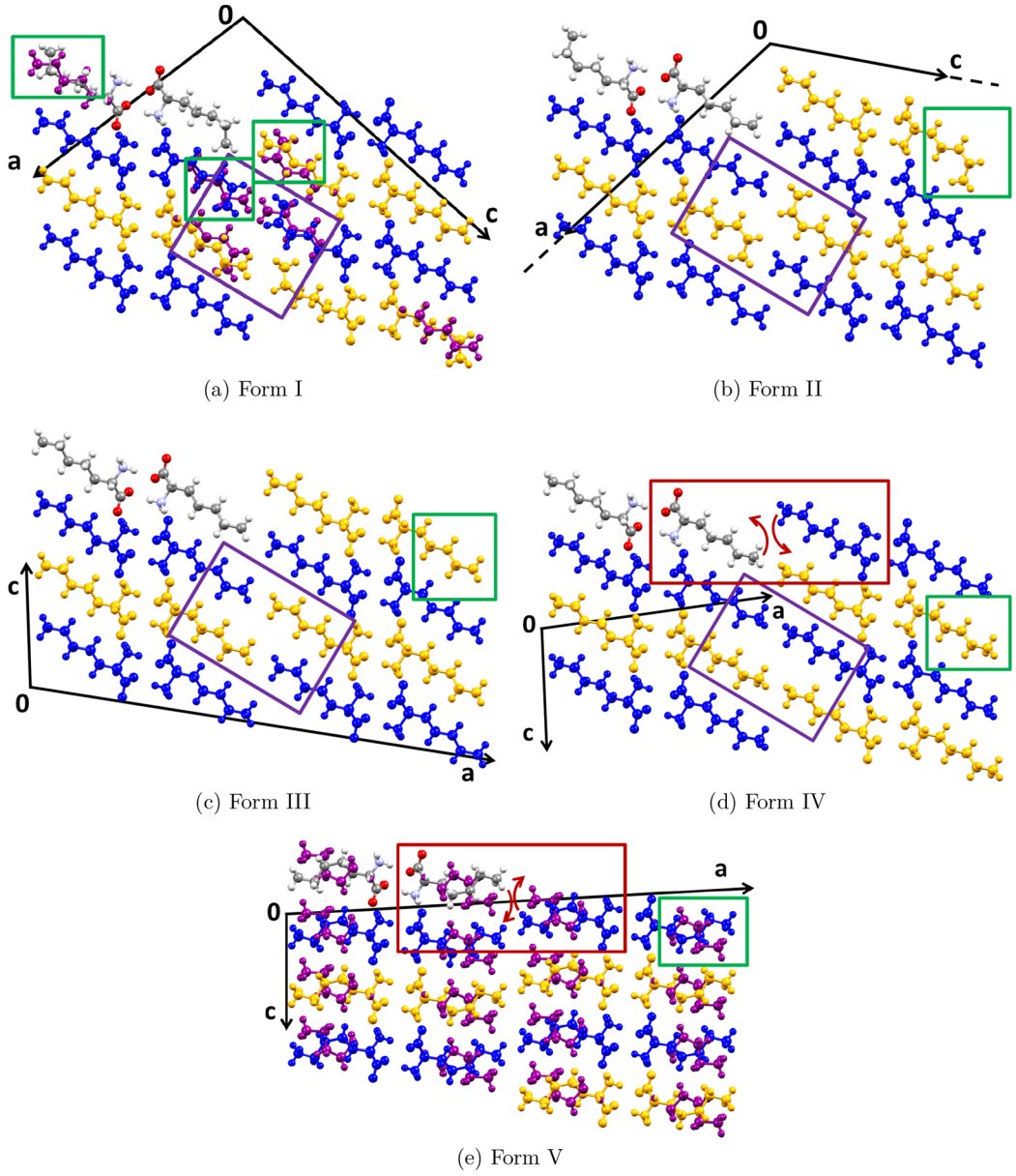

Figure 3. DL-AHE crystal structures of the five polymorphic forms (a) I, (b) II, (c) III, (d) IV, and (e) V, drawn in the *ac*-plane of form IV for comparison. L-AHE molecules (absolute configuration *S*) are depicted in yellow, D-AHE molecules in blue. The green boxes indicate differences in conformation of the aliphatic chains, and purple and red boxes indicate the relative positions of the bilayers.

transition and the reversibility and reproducibility. A typical DSC curve of DL-AHE between 133 and 423 K shows two endothermic events during heating and two exothermic events during cooling, both in powder and single crystals, and is shown for a powder in Figure 5a. Following the SCXRD results, three solid-state phase transitions should occur in this temperature range. All events are reproducible and in accordance with the "heat-of-transition rule".[37] Two reversible solid-state phase transitions occur at 146 and 396 K, both with a small hysteresis of 1−2 K. The transitions have been identified as the II ↔ III transition at 146 K and the IV ↔ V transition at 396 K, for which the enthalpies of transition are 0.8 ± 0.1 kJ/mol and 2.8 ± 0.3 kJ/mol, respectively. The small hysteresis and the similar magnitude of the enthalpy measured during heating and cooling of the same transition show that these two transitions are thermodynamically reversible and not kinetically hindered. The III ↔ IV transition is only visible in single crystals using a heating rate of 5 K/min or higher, as a very low intensity broad signal at 213 K during cooling and 223 K during heating with a $\Delta H < 0.04$ kJ/mol, as is shown in Figure 5b. This phase transition is similar to the $\beta \leftrightarrow \alpha$ phase transition in DL-NLE, there we have attributed the large hysteresis to the small driving force for the phase transition.[5] The other phase transitions all involve conformational changes of the molecules and thus larger transition enthalpies, which leads to a larger driving force just above or below the transition point and therefore a small hysteresis. The transition temperatures are in accordance with the SCXRD results in Figure 2.

3.3. Thermal Stage Polarization Microscopy. Single crystals of DL-AHE have been monitored as a function of temperature using thermal stage polarization microscopy, snapshots of which are shown in Figure 6. The snapshots are compiled as a video capture in the file Movie S1 in the Supporting Information. The high temperature IV ↔ V phase transition is clearly observed as motions of the whole crystal or its separate

DOI: 10.1021/acs.cgd.7b01175
Cryst. Growth Des. 2018, 18, 242−252

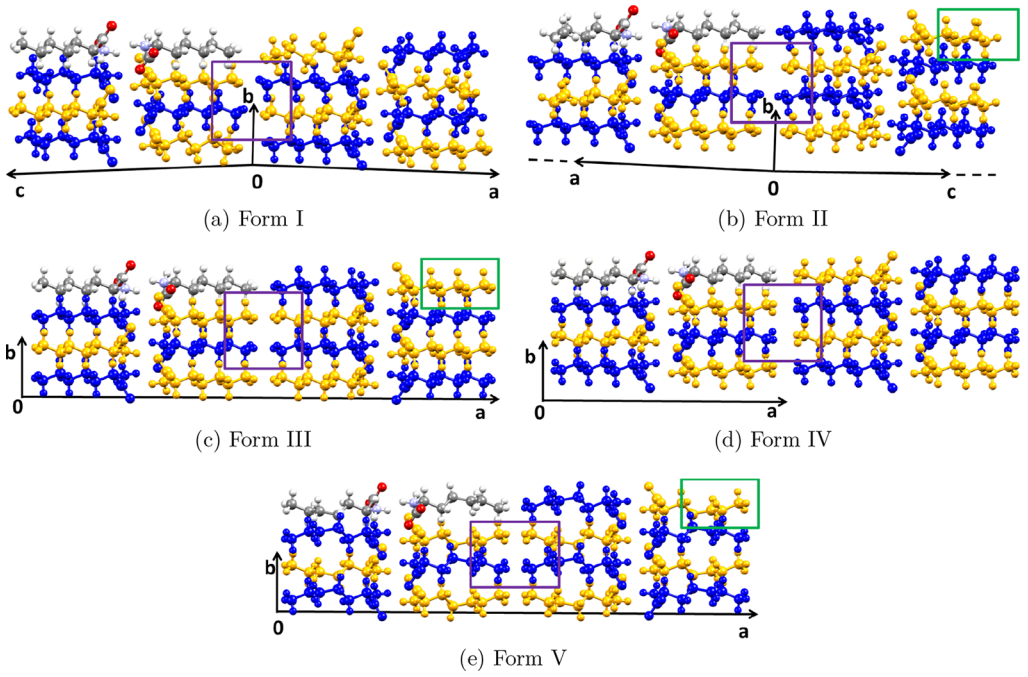

Figure 4. DL-AHE crystal structures of the five polymorphic forms (a) I, (b) II, (c) III, (d) IV, and (e) V, only one conformation of forms I and V is shown), drawn in the *ab*-plane of form IV for comparison. L-AHE molecules (absolute configuration *S*) are depicted in yellow, D-AHE molecules in blue. The green boxes indicate differences in conformation of the aliphatic chains, and purple boxes indicate the relative positions of the bilayers.

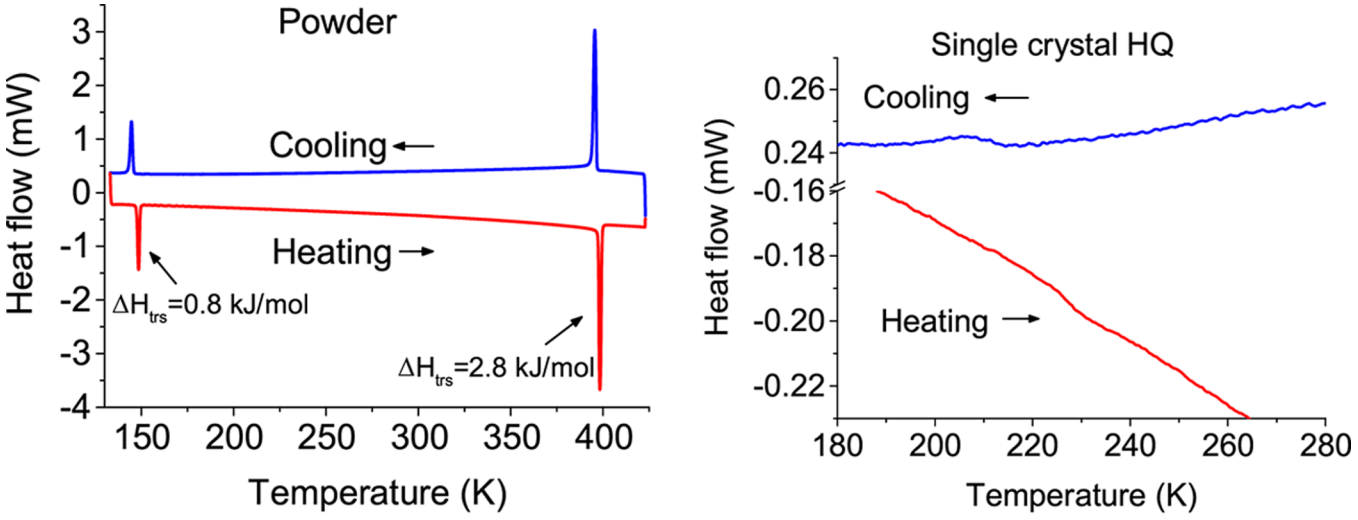

Figure 5. DSC thermograms of DL-AHE (a) powder (6.2 mg) between 133 to 433 K, showing the II ↔ III transition at 146 K and the IV ↔ V transition at 396 K at a heating rate of 2 K/min, (b) two single crystals (1.4 mg) showing the III ↔ IV transition between 213 and 223 K at a heating rate of 5 K/min. The transitions were reversible and repeatable, both in powder and single crystals.

layered parts. In addition, there is a change in the polarization color, which often occurs as several consecutive color changes for the different layers in the crystal. In some cases a transition front within the plane of a layer is observed, originating from a visible defect, but mostly the transition appears to be instantaneous in a layer using a frame rate of 3 Hz. This fast propagation within a layer indicates possible cooperative motion. To accommodate the conformational changes in a cooperative mechanism, we suggest a "pedal crank"-type mechanism. The transition occurs at about 397 K, with a small variation in transition temperature between different crystals, and it is fast and repeatable. No visible delamination or deterioration of the crystallinity occurs. There is a small hysteresis between the heating and cooling cycles of about 1 K.

The low temperature II ↔ III transition is less apparent, though in most crystals it can be observed as a small change in polarization color and in some cases as motions of the whole crystal or a few layers, see Movie S2 in the Supporting Information. The phase transition occurs at about 146 K, with some variation in transition temperature between different crystals, and it can be spread out over 10−20 K within one crystal. This is probably a result of slow kinetics at these low temperatures, since there is only a small hysteresis between the heating and cooling cycles of about 1−2 K in most cases.

DOI: 10.1021/acs.cgd.7b01175
Cryst. Growth Des. 2018, 18, 242−252

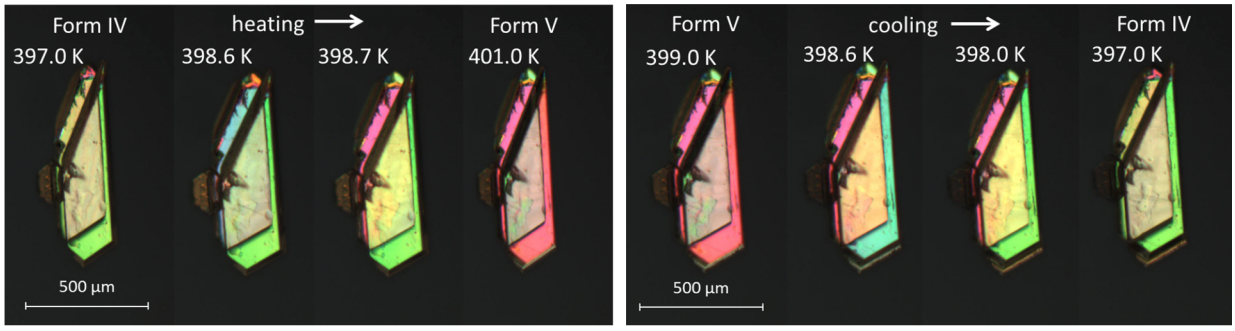

Figure 6. Thermal microscopy images of the phase transitions of DL-AHE; (a) the IV → V phase transition, and (b) the V → IV phase transition at 397 K.

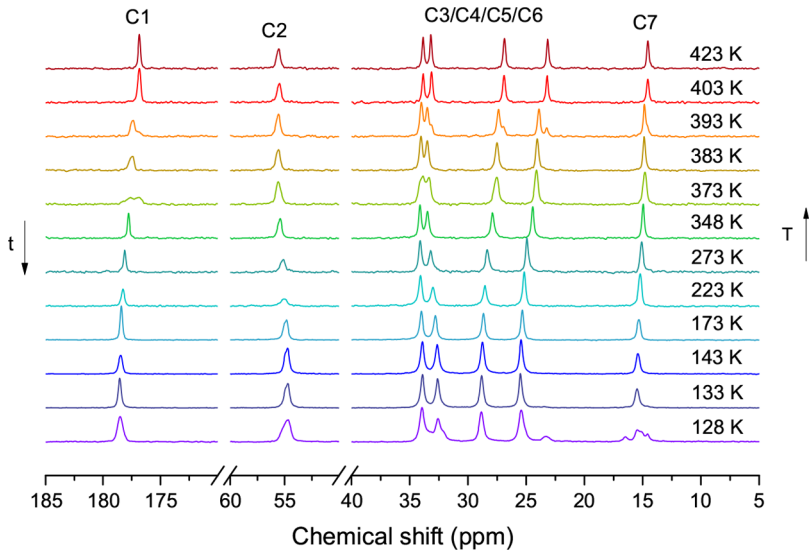

Figure 7. ^{13}C CPMAS NMR spectra of a powder sample of DL-AHE during cooling from 423 to 128 K. The V → IV phase transition occurs between 403 and 383 K, and it involves a change in chemical shift of all peaks except C2. The IV → III transition is not detectable. The broadening of the peaks at 128 K clearly shows the onset of the III → II transition.

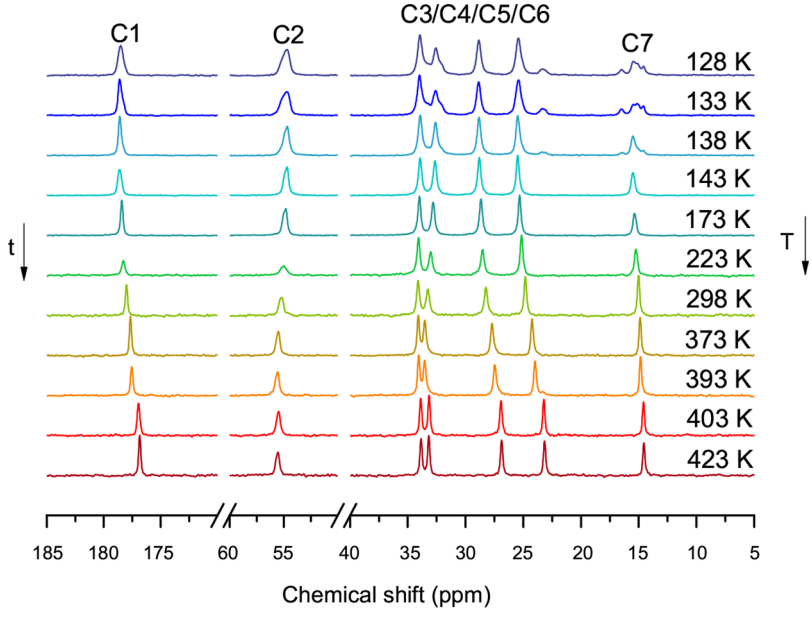

Figure 8. ^{13}C CPMAS NMR spectra of a powder sample of DL-AHE during heating from 128 to 423 K. The narrowing of the peaks between 138 and 143 K shows the II → III transition. The III → IV transition is not detectable. The IV → V phase transition occurs between 393 and 403 K and it involves a change in chemical shift of all peaks except C2.

DOI: 10.1021/acs.cgd.7b01175
Cryst. Growth Des. 2018, 18, 242−252

There was no clear indication of the III ↔ IV phase transition in our thermal stage microscopy measurements, although several very small movements can be observed at various temperatures (see Movie S2 in the Supporting Information) that might indicate partial transitions. This phase transition is very subtle and almost too weak for optical detection.

3.4. Solid-State NMR. Solid-state NMR can reveal small differences in the local environment of the carbon atoms, showing the coexistence of phases and differences between similar crystal structures. The solid-state NMR spectra of DL-AHE (Figures 7 and 8) show the II ↔ III and IV ↔ V phase transitions between 128 and 143 K and 383−403 K, respectively. The III ↔ IV phase transition is not detectable, as is shown in more detail further on. The high temperature IV ↔ V phase transition is observed as a change in the chemical shift of all carbon atoms, except C2, with the largest shift in C6. The transition is fast, and coexistence of both phases is only visible at 393 K during cooling, and could even be a result of a temperature gradient in the sample. The II ↔ III transition is observed as an increase of the number of distinct chemical environments for each carbon atom upon cooling, indicated by severe line broadening. This is most clearly observable in the signal of C6 and C7, for which at least two (C6) and four (C7) distinct peaks can be distinguished, respectively. This phase transition showed no significant hysteresis in DSC measurements, both for powders and single crystals. However, the transition temperature is close to the limit of what can be achieved for the NMR probe used, and therefore the temperature control is slightly less accurate and there is some lag in the actual temperature of the whole sample, since the cooling is done using a nitrogen gas flow.

Forms III, IV, and V all have $Z' = 1$, thus generating only one chemical environment for each distinct atom. However, the asymmetric unit of form II consists of eight molecules, with each a distinct chemical environment. This is illustrated by Figure 9,

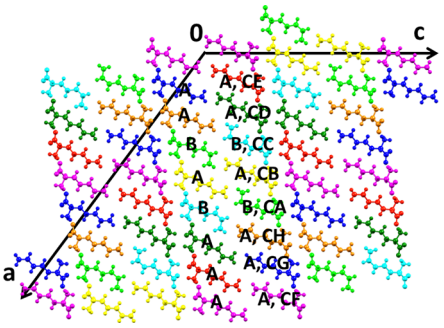

Figure 9. Crystal structure of form II of DL-AHE, depicted in the *ac*-plane, showing the eight different molecules (CA to CH) in the asymmetric unit in distinct colors. A and B indicate the two distinct conformations of the molecules.

where nonsymmetry-equivalent molecules are represented by eight different colors within the unit cell for form II. First of all, two conformations can be distinguished; conformation A of the yellow (CB), dark-green (CD), red (CE), pink (CF), dark-blue (CG), and orange (CH) molecules, and conformation B of the light-green (CA) and light-blue (CC) molecules in Figure 9.

The assignment of the ^{13}C NMR peaks to the carbon atoms in the unit cell was derived from density functional theory (DFT) calculations. Figure 10a,b both show in black the total calculated NMR spectrum of form II and in colors the calculated peaks originating from conformation A (Figure 10a) and conformation

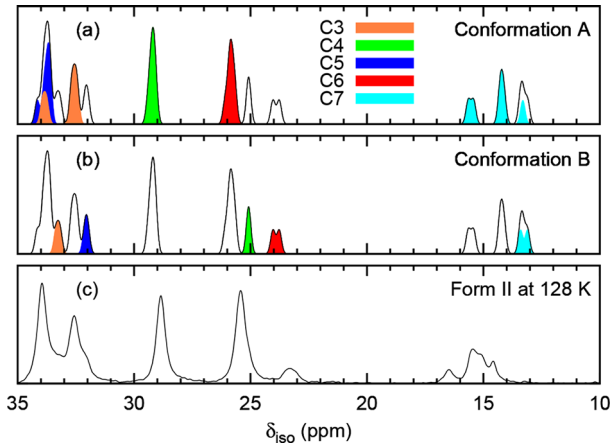

Figure 10. Comparison of the DFT calculations and the ^{13}C CPMAS NMR spectrum of DL-AHE form II for C3, C4, C5, C6, and C7. The chemical shift values from the DFT calculations for (a) the A and (b) the B conformations of DL-AHE II are depicted. The black lines in (a) and (b) show the total calculated NMR spectrum, assuming equal weight and width for each contributing C. The colored peaks show the contribution of conformation A (a) and B (b) to this spectrum. Adding all contributions from all colored peaks from both A and B yields the total (black line) (c). The experimental ^{13}C NMR spectrum of form II measured at 128 K.

B (Figure 10b). The calculated NMR spectrum is shown with a sum of gaussians with fwhm = 0.24 pmm at the calculated chemical shifts. For comparison, Figure 10c shows the experimental NMR spectrum of form II at 128 K.

The two peaks of C6 belong to the two different conformations present in form II, the corresponding values are 25.4 and 23.3 ppm for conformation A and B, respectively. Moreover, the order of the chemical shift peaks is different from what would be expected based on the NMR spectra of the similar amino acid DL-NLE.[5] In DL-NLE, when moving along the chain toward the terminal CH_3, the ^{13}C chemical shift always increases. This is not the case here, where the C3 and C5 have lower shifts than the C4 and C6. The positions of the C3 and C5 peaks are exchanged in the A and B conformations, and the C4 peak of conformation A is in between the C3/C5 and C6 positions. Additionally, the C4 peak of conformation B overlaps with the C6 of conformation A according to the calculations. The ^{13}C NMR chemical shifts calculated by DFT are shown for each separate molecule in the asymmetric unit in the Supporting Information.

According to the DFT calculations (see Supporting Information for more details), the red (CE) and pink (CF) molecules of form II have chemical shifts most similar to form III. These molecules and their direct neighbors in the unit cell are all of conformation A, which is the same conformation as is present in form III. Both contribute to the middle C7 peak at 14.3 ppm. We identify this with the experimental peak at 15.5 ppm, which has the highest relative intensity of the four peaks. Furthermore, the light-green (CA) and light-blue (CC) molecules are both of conformation B, and all their direct neighbors are of conformation A. This apparently results in a similar chemical shift for both B molecules at 13.3 ppm, which corresponds to the experimental C7 at 14.6 ppm. The other molecules of the A conformation have at least one B molecule as a (nearest) neighbor. Since the distance to the directly opposite neighbor is the smallest, this is considered to have the largest effect on the chemical shift. However, the position of the C7 peak for the other

DOI: 10.1021/acs.cgd.7b01175
Cryst. Growth Des. 2018, 18, 242−252

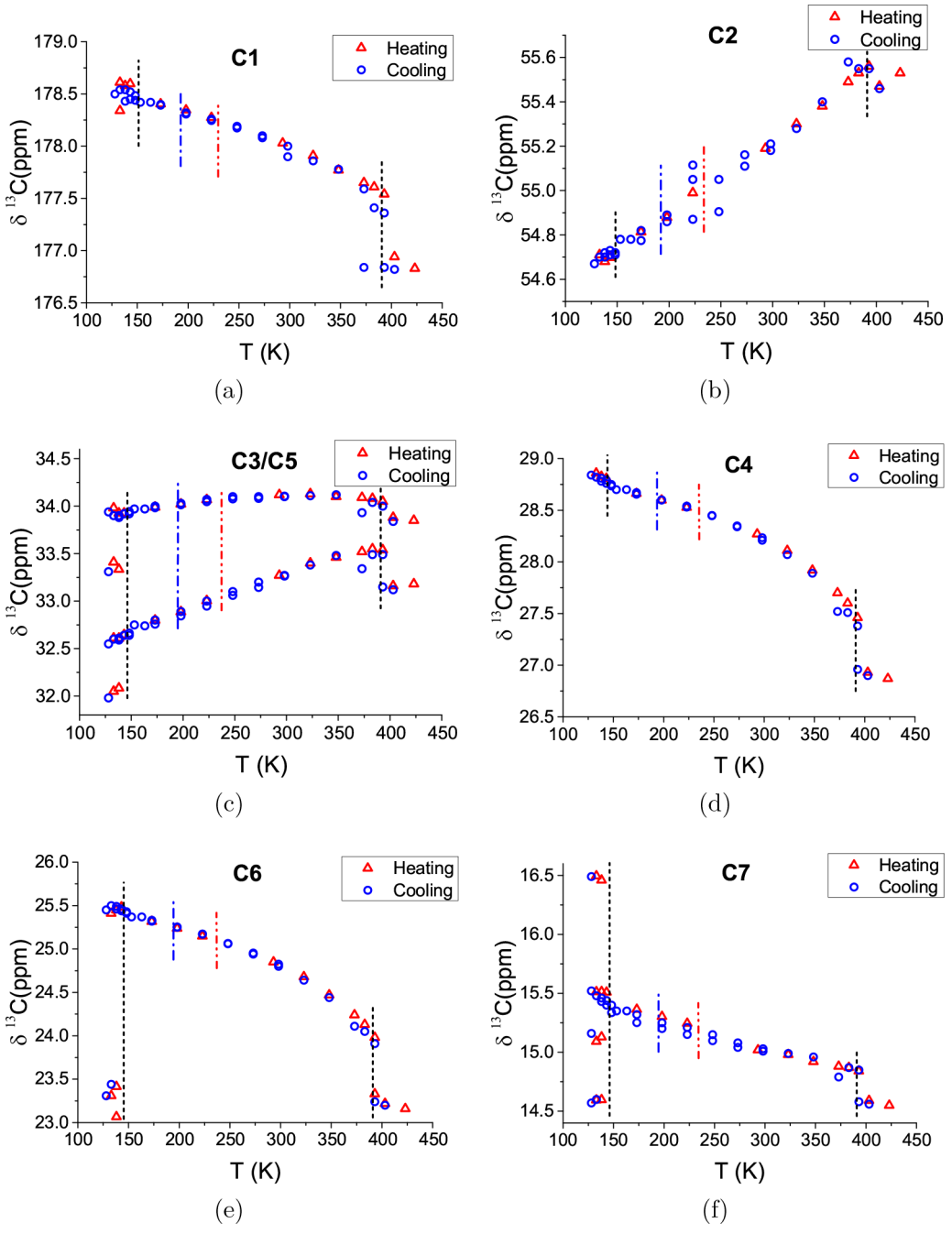

Figure 11. ^{13}C Chemical shift of DL-AHE as a function of temperature for a powder sample. The dashed lines indicate the phase transition temperatures observed in SCXRD measurements (Figure 2) for forms II ↔ III (black), for III ↔ IV during cooling (blue) and heating (red), and for IV ↔ V (black).

molecules is not clearly related to the nature of the opposite neighbor. The C7 position of the orange (CH) molecule even overlaps with the positions of the B molecules according to the DFT calculations, which is unexpected. Therefore, our assignment of the eight molecules to the observed C7 spectrum is not unambiguous.

In summary, the observed splitting of the chemical shift in the solid-state NMR spectra confirms the increase of Z' during the III → II transition, and this is supported by DFT calculations.

The chemical shift as a function of temperature for all carbon atoms is shown in Figure 11 for a powder sample. Measurements of single crystals did not show significant differences compared to powder samples. Again, the II ↔ III and IV ↔ V phase transitions can be clearly recognized by the discontinuity in the value of the chemical shift of several carbon atoms. This is indicated by the black dashed lines that correspond to the temperatures at which the phase transitions were observed in SCXRD measurements depicted in Figure 2. The III ↔ IV phase transition is not clearly visible, only a gradual change in the slope of the chemical shift as a function of temperature can be seen, which might be a result of this transition. The observed phase transition temperatures in SCXRD are shown for the III ↔ IV phase transition during cooling (blue) and heating (red), but no well-defined change in the slope has been observed at these temperatures.

The chemical shift difference of the high temperature IV ↔ V phase transition is only 0.5 and 0.3 ppm for C6 and C7, respectively, although it involves both a shift and a conformational change. Also, only one set of peaks is observed for form V,

DOI: 10.1021/acs.cgd.7b01175
Cryst. Growth Des. 2018, 18, 242−252

although the crystal structure shows two conformations with relatively high occupancies. Possibly, the disorder in conformation is dynamic and averages out during the NMR measurements.

3.5. Comparison with DL-Norleucine. The three polymorphic forms of DL-norleucine (DL-2-aminohexanoic acid, DL-NLE), described in detail in refs 4 and 5 have very similar structures to three of the polymorphs of DL-AHE. The β form of DL-NLE is stable at low temperatures, the α form at room temperature and the γ form at high temperatures. Here, we compare the crystal structures and the solid-state phase transition behaviors of DL-AHE and DL-NLE.

The low temperature DL-AHE III ↔ IV and the DL-NLE $\beta \leftrightarrow \alpha$ phase transitions both involve the same shift over [0 $^1/_2$ $^1/_2$] in the packing of the bilayers (compare the contents of the purple boxes in Figures 3c,d and 4c,d), no conformational change nor any significant volume change. While the DL-NLE $\beta \leftrightarrow \alpha$ phase transition has an estimated enthalpy of only 0.3 kJ/mol and is difficult to reproduce, the DL-AHE III ↔ IV phase transition has an even lower transition enthalpy of 0.04 kJ/mol, but it is reproducible at heating rates above 5 K/min. The corresponding transition temperatures are 253−268 K and 213−223 K, respectively. These transitions have an overall low transition rate, since different domains of layers transform independently. Increased chain mobility in the longer aliphatic chains of DL-AHE weakens the interactions between the chains on opposite sides of a bilayer−bilayer interface, probably resulting in a smaller transition enthalpy and a lower transition temperature for this type of transition.

The high temperature DL-AHE IV ↔ V and the DL-NLE $\alpha \leftrightarrow \gamma$ phase transitions both involve a packing and a conformational change. These phase transitions are relatively fast and reproducible with a small hysteresis. Similar to the low temperature phase transitions, the transition enthalpy of DL-NLE $\alpha \leftrightarrow \gamma$ is significantly higher than of DL-AHE IV ↔ V, 4.8 and 2.8 kJ/mol, respectively. The transition temperatures are quite similar, 390 and 396 K, respectively. In addition, the solid-state NMR measurements show that the chemical shift differences of terminal carbon atom (C6) for the DL-NLE phase transitions are significantly larger than for DL-AHE (C7); 0.4 vs <0.1 ppm for the low temperature transitions and 0.8 vs 0.3 ppm for the high temperature transitions. Again, we think that the increased chain mobility further reduces the strength of the weak interactions between the layers, thereby resulting in smaller enthalpy and chemical shift differences between the polymorphic forms.

Other effects can also play a role, especially in the comparison of the high temperature transitions. First, the torsion angle that changes for one of the two form V conformations in the DL-AHE IV↔V transition is positioned more toward the end of the aliphatic chain than for the DL-NLE $\alpha \leftrightarrow \gamma$ transition, which decreases the impact of the phase transition on the initial structure compared to DL-NLE. Second, the shift in packing is in a different direction and covers a shorter distance than in DL-NLE. Furthermore, the NMR chemical shifts of different conformations in form V could be averaged out due to high mobility. Lastly, the carbon chain length is odd for DL-AHE and even for DL-NLE, which influences the mutual orientation of the aliphatic chains and could influence the energy barrier for the rearrangement of the bilayers.

4. CONCLUSIONS

The rich polymorphic landscape and the solid-state phase transitions of DL-aminoheptanoic acid (DL-AHE) have been studied in detail. Five new polymorphic forms and four fully reversible single-crystal-to-single-crystal solid-state phase transitions between these forms have been discovered. In general, the crystal structures show great similarity to other racemic amino acids with a linear (unbranched) aliphatic chain, consisting of bilayers based on a 2D LD−LD hydrogen bonding network and dispersive interactions between the aliphatic chains. The low temperature forms I and II of DL-AHE are superstructures, which had not been observed up to now in linear racemic amino acids; the crystal structures were refined as high Z' structures ($Z' = 6$ and $Z' = 8$, respectively). The increase in Z' is confirmed by solid-state NMR measurements. DFT calculations of the NMR chemical shift showed an unexpected assignment of the NMR spectrum to the carbon atoms of DL-AHE.

The increased chain length of DL-AHE results in increased chain mobility of the aliphatic chains, which weakens the interactions between the chains on opposite sides of a bilayer−bilayer interface. Therefore, the enthalpies of transition and the ^{13}C chemical shift differences of the solid-state phase transitions in DL-AHE are much smaller than for the related transitions in DL-norleucine (DL-NLE). This multidisciplinary study shows that a combination of techniques is necessary to optimally cover the experimental polymorphic landscape. Weak interactions within the crystal structure allow for very subtle solid-state phase transitions that can easily be overlooked.

■ ASSOCIATED CONTENT

Supporting Information

The Supporting Information is available free of charge on the ACS Publications website at DOI: 10.1021/acs.cgd.7b01175.

DFT calculations of the ^{13}C CPMAS NMR spectrum of DL-2-aminoheptanoic acid form II for C3, C4, C5, C6, and C7 (PDF)

Video recordings of optical microscopy observations of single crystals showing the solid-state phase transitions; Movies S1 (MP4-1) and S2 (MP4-2)

Accession Codes

CCDC 1563210−1563214 (corresponding to the five crystal structures of DL-AHE) contain the supplementary crystallographic data for this paper. These data can be obtained free of charge via www.ccdc.cam.ac.uk/data_request/cif, or by emailing data_request@ccdc.cam.ac.uk, or by contacting The Cambridge Crystallographic Data Centre, 12 Union Road, Cambridge CB2 1EZ, UK; fax: +44 1223 336033.

■ AUTHOR INFORMATION

Corresponding Authors

*(S.J.C.) E-mail: s.j.coles@soton.ac.uk.
*(H.M.C.) E-mail: h.cuppen@science.ru.nl.

ORCID

Mireille M. H. Smets: 0000-0003-1938-2099
Gilles A. de Wijs: 0000-0002-1818-0738
Elias Vlieg: 0000-0002-1343-4102

Notes

The authors declare no competing financial interest.

DOI: 10.1021/acs.cgd.7b01175
Cryst. Growth Des. 2018, 18, 242−252

■ ACKNOWLEDGMENTS

The authors are grateful for financial support from the VIDI research program 700.10.427 financed by the Dutch Organisation for Scientific Research (NWO) and the ERC grant from the European Research Council (ERC-2010-StG, Grant Agreement 259510-KISMOL). Support of the Dutch Organisation for Scientific Research (NWO) for the solid-state NMR facility for advanced materials science in Nijmegen is gratefully acknowledged. We are also grateful to the UK Engineering and Physical Sciences Research Council for funding the National Crystallography Service under its National Research Facilities programme. We acknowledge Diamond Light Source for time on beamline I-19 under Proposal MT6916. We thank G. Janssen, H. Janssen, and J. Schoonbrood for support with the solid-state NMR measurements and Erik de Ronde for other technical support. Furthermore, we thank the anonymous referee for providing us with an improved structure refinement of form V, which was used as input for our final crystal structure refinement.

■ REFERENCES

(1) Görbitz, C. H.; Alebachew, F.; Petříček, V. Solid-State Phase Transitions of DL-Aminobutyric Acid. *J. Phys. Chem. B* **2012**, *116*, 10715−10721.
(2) Ren, P.; Reichert, D.; He, Q.; Zhang, L.; Tang, H. Understanding the Molecular Dynamics Associated with Polymorphic Transitions of DL-Norvaline with Solid-State NMR Methods. *J. Phys. Chem. B* **2011**, *115*, 2814−2823.
(3) Görbitz, C. H. Solid-State Phase Transitions in DL-Norvaline Studied by Single-Crystal X-ray Diffraction. *J. Phys. Chem. B* **2011**, *115*, 2447−2453.
(4) Coles, S. J.; Gelbrich, T.; Griesser, U. J.; Hursthouse, M. B.; Pitak, M.; Threlfall, T. The Elusive High Temperature Solid-State Structure of D,L-Norleucine. *Cryst. Growth Des.* **2009**, *9*, 4610−4612.
(5) Smets, M. M. H.; Brugman, S. J. T.; van Eck, E. R. H.; van den Ende, J. A.; Meekes, H.; Cuppen, H. M. Understanding the Solid-State Phase Transitions of DL-Norleucine: An in Situ DSC, Microscopy, and Solid-State NMR Study. *Cryst. Growth Des.* **2015**, *15*, 5157−5167.
(6) Görbitz, C. H.; Paulsen, J. C.; Borgersen, J. Redetermined crystal structure of β-DL-methionine at 320K. *Acta Cryst. Sect. E* **2015**, *71*, o398−o399.
(7) Smets, M. M. H.; Brugman, S. J. T.; van Eck, E. R. H.; Tinnemans, P.; Meekes, H.; Cuppen, H. M. Understanding the single-crystal-to-single-crystal solid-state phase transition of DL-methionine. *CrystEngComm* **2016**, *18*, 9363−9373.
(8) Van den Ende, J. A.; Ensing, B.; Cuppen, H. M. Energy barriers and mechanisms in solid-solid polymorphic transitions exhibiting cooperative motion. *CrystEngComm* **2016**, *18*, 4420−4430.
(9) Coles, S. J.; Gale, P. A. Changing and challenging times for service crystallography. *Chem. Sci.* **2012**, *3*, 683−689.
(10) *CrystalClear-SM Expert 3.1 b27*; Rigaku Oxford Diffraction, 2012.
(11) , *CrysAlisPro 1.171.38.41*; Rigaku Oxford Diffraction, 2015.
(12) Sheldrick, G. M. A short history of *SHELX*. *Acta Crystallogr., Sect. A: Found. Crystallogr.* **2008**, *64*, 112−122.
(13) Sheldrick, G. M. Crystal structure refinement with *SHELXL*. *Acta Crystallogr., Sect. C: Struct. Chem.* **2015**, *71*, 3−8.
(14) Dolomanov, O. V.; Bourhis, L. J.; Gildea, R. J.; Howard, J. A. K.; Puschmann, H. *OLEX2:* a complete structure solution, refinement and analysis program. *J. Appl. Crystallogr.* **2009**, *42*, 339−341.
(15) Fung, B.; Khitrin, A.; Ermolaev, K. An Improved Broadband Decoupling Sequence for Liquid Crystals and Solids. *J. Magn. Reson.* **2000**, *142*, 97−101.
(16) van Beek, J. D. matNMR: A flexible toolbox for processing, analyzing and visualizing magnetic resonance data in Matlab. *J. Magn. Reson.* **2007**, *187*, 19−26.
(17) Kresse, G.; Hafner, J. Ab initio. *Phys. Rev. B: Condens. Matter Mater. Phys.* **1993**, *47*, 558−561.
(18) Kresse, G.; Furthmüller, J. Efficient iterative schemes for ab initio total-energy calculations using a plane-wave basis set. *Phys. Rev. B: Condens. Matter Mater. Phys.* **1996**, *54*, 11169−11186.
(19) Blöchl, P. E. Projector augmented-wave method. *Phys. Rev. B: Condens. Matter Mater. Phys.* **1994**, *50*, 17953−17979.
(20) Kresse, G.; Joubert, D. From ultrasoft pseudopotentials to the projector augmented-wave method. *Phys. Rev. B: Condens. Matter Mater. Phys.* **1999**, *59*, 1758−1775.
(21) Perdew, J. P.; Burke, K.; Ernzerhof, M. Generalized Gradient Approximation Made Simple. *Phys. Rev. Lett.* **1996**, *77*, 3865−3868.
(22) Perdew, J. P.; Burke, K.; Ernzerhof, M. Generalized Gradient Approximation Made Simple[Phys. Rev. Lett. 77, 3865 (1996)]. *Phys. Rev. Lett.* **1997**, *78*, 1396−1396.
(23) Grimme, S.; Antony, J.; Ehrlich, S.; Krieg, H. A consistent and accurate ab initio parametrization of density functional dispersion correction (DFT-D) for the 94 elements H-Pu. *J. Chem. Phys.* **2010**, *132*, 154104.
(24) Pickard, C. J.; Mauri, F. All-electron magnetic response with pseudopotentials: NMR chemical shifts. *Phys. Rev. B: Condens. Matter Mater. Phys.* **2001**, *63*, 245101.
(25) Yates, J. R.; Pickard, C. J.; Mauri, F. Calculation of NMR chemical shifts for extended systems using ultrasoft pseudopotentials. *Phys. Rev. B: Condens. Matter Mater. Phys.* **2007**, *76*, 024401.
(26) de Wijs, G. A.; Laskowski, R.; Blaha, P.; Havenith, R. W. A.; Kresse, G.; Marsman, M. NMR shieldings from density functional perturbation theory: GIPAW versus all-electron calculations. *J. Chem. Phys.* **2017**, *146*, 064115.
(27) Kresse, G., Marsman, M., Furthmüller, J. VASP The guide, 2015; http://cms.mpi.univie.ac.at/marsweb.
(28) King-Smith, R. D.; Payne, M. C.; Lin, J. S. Real-space implementation of nonlocal pseudopotentials for first-principles total-energy calculations. *Phys. Rev. B: Condens. Matter Mater. Phys.* **1991**, *44*, 13063−13066.
(29) Görbitz, C. H.; Qi, L.; Mai, N. T. K.; Kristiansen, H. Redetermined crystal structure of α-DL-methionine at 340K. *Acta Crystallogr., Sect. E: Struct. Rep. Online* **2014**, *70*, 337−340.
(30) Görbitz, C. H.; Vestli, K.; Orlando, R. A solution to the observed $Z' = 2$ preference in the crystal structures of hydrophobic amino acids. *Acta Crystallogr., Sect. B: Struct. Sci.* **2009**, *65*, 393−400.
(31) Braun, D. E.; Krüger, H.; Kahlenberg, V.; Griesser, U. J. Molecular Level Understanding of the Reversible Phase Transformation between Forms III and II of Dapsone. *Cryst. Growth Des.* **2017**, *17*, 5054−5060.
(32) Day, G. M.; Cooper, T. G. Crystal packing predictions of the alpha-amino acids: methods assessment and structural observations. *CrystEngComm* **2010**, *12*, 2443−2453.
(33) Görbitz, C. H.; Dalhus, B.; Day, G. M. Pseudoracemic amino acid complexes: blind predictions for flexible two-component crystals. *Phys. Chem. Chem. Phys.* **2010**, *12*, 8466−8477.
(34) Fábián, L.; Brock, C. P. A list of organic kryptoracemates. *Acta Crystallogr., Sect. B: Struct. Sci.* **2010**, *66*, 94−103.
(35) Dalhus, B.; Görbitz, C. H. Non-centrosymmetric racemates: space-group frequencies and conformational similarities between crystallographically independent molecules. *Acta Crystallogr., Sect. B: Struct. Sci.* **2000**, *56*, 715−719.
(36) Groom, C. R.; Bruno, I. J.; Lightfoot, M. P.; Ward, S. C. The Cambridge Structural Database. *Acta Crystallogr., Sect. B: Struct. Sci., Cryst. Eng. Mater.* **2016**, *72*, 171−179.
(37) Burger, A.; Ramberger, R. On the polymorphism of pharmaceuticals and other molecular crystals. I. *Microchim. Acta* **1979**, *72*, 259−271.

DOI: 10.1021/acs.cgd.7b01175
Cryst. Growth Des. 2018, 18, 242−252